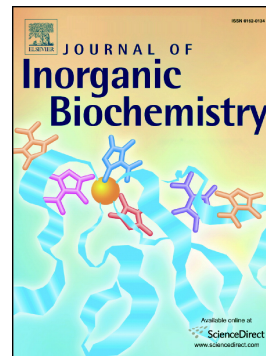# Journal Pre-proof

Alcian blue pyridine variant interaction with DNA and RNA polynucleotides and G-quadruplexes: Changes in the binding features for different biosubstrates

Francesca Macii, Cristina Perez Arnaiz, Lorenzo Arrico, Natalia Busto, Begona Garcia, Tarita Biver

Alcian blue pyridine variant interaction with DNA and RNA polynucleotides and G-quadruplexes: changes in the binding features for different biosubstrates

Francesca Macii,[1] Cristina Perez Arnaiz,[2] Lorenzo Arrico,[1] Natalia Busto,[2] Begona Garcia,[2] Tarita Biver[3,1*]

[1] Department of Chemistry and Industrial Chemistry, University of Pisa, Via G. Moruzzi 13, 56124 Pisa, Italy

[2] Department of Chemistry, University of Burgos, Pza. Misael Bañuelos s/n, 09001 Burgos, Spain

[3] Department of Pharmacy, University of Pisa, Via Bonanno Pisano 6, 56126 Pisa, Italy, tarita.biver@unipi.it

Keywords

Groove binding, partial intercalation, helix conformation, enthalpy-entropy compensation, anti-parallel, hybrid

Abstract

This work concerns an analysis of the binding mechanism of a copper phthalocyanine (Alcian Blue-tetrakis(methylpyridinium) chloride, ABTP) to natural calf thymus DNA, G-quadruplexes (G4) and synthetic RNA polynucleotides in the form of double polyriboadenylic·polyribouridylic acid (poly(A)·poly(U)) or triple strands polyriboadenylic·2polyribouridylic acid (poly(A)·2poly(U)). ABTP is a well know dye that might undergo novel applications, but its interaction with DNA is scarcely studied and we lack information on possible RNA or G4 binding. This might be related to system complexity due to the presence of supramolecular dye-dye aggregates. Despite this, we show here that apparent parameters can be calculated, which provide information on the binding mechanism. Absorbance titrations in the presence of biosubstrate excess, melting and circular dichroism experiments show that ABTP binds to both RNAs and DNA. External/groove binding is the main feature for RNAs, whereas partial intercalation is the major binging mode for DNA. ABTP externally binds to both hybrid, parallel and anti-parallel G4s but seem to show a slightly different binding mode and a preference for anti-parallel structures. The thermodynamic features of the different systems are also discussed in the frame of the enthalpy-entropy compensation phenomenon.

Introduction

Phthalocyanines are aromatic compounds composed of four isoindole rings connected by nitrogen atoms which can form stable metal complexes upon the double deprotonation of the isoindole groups. The peripheral rings can also bear different substituents, whose features modulate the photophysical properties of the dye, together with the metal centre. Thus, the absorption and emission properties of phthalocyanines can be tuned to obtain different coloured dyes and pigments. It is estimated that approximately 25% of all artificial organic pigments are phthalocyanine derivatives [1]. Among others, Cu(II) phthalocyanines are widely exploited as bright blue pigments in paints, printing inks and textile dyeing [2]. Moreover, these Cu(II) complexes have been historically used as markers in histologic staining methods. Alcian Blue is considered one of the most common dye for staining tissues, thanks to its affinity for polysaccharides [3].

Although Alcian Blue undoubtedly presents suitable features (i.e. aromatic structure and cationic substituents) to bind polynucleotides, its interaction with DNA is scarcely studied and, to the best of our knowledge, no information on the binding to RNA polynucleotides is known. The very first obstacle was certainly the lack of structural information until 1973 [4]. Pioneering work by Scott affirmed that Alcian Blue does bind DNA through electrostatic forces, but the steric hindrance caused by the peripheral groups prevents the insertion of the dye into the stacked base pairs [5]. Since then, at the best of our knowledge, no mechanistic study had been performed and detailed information on the reactivity towards bio-substrates is missing in the literature. Also, it should be noted that Alcian Blue is highly prone to self-aggregate in water solution [6] and the formation of supramolecular aggregates surely limits the direct interaction with the polynucleotide and complicates its analysis. The lack of information clashes with the increasing biomedical role of phthalocyanines, which have recently gained high interest as widely diffused

therapeutical agents. For example, phthalocyanines are extensively studied and employed as photosensitizers for photodynamic therapy thanks to their suitable photophysical properties [7-9]. Also, recent researches have been focusing on the potential anticancer activity of these compounds [8, 10-13]. Among other non-canonical polynucleotides forms, G-quadruplex DNA structures (G4) have received widespread attention because of their involvement in the mortality of the cancer cells [14]. Ligands that stabilize or induce the formation of G4 structures can be considered as promising anticancer agents [15]. The structural features of phthalocyanines should allow the molecules to bind to human G-quadruplex DNA with high affinity through π-π stacking interactions [16, 17].

On the above basis, the presented work concerns the study of the interaction between nucleic acids and Alcian Blue-tetrakis(methylpyridinium) chloride (ABTP, Figure 1), which is a Cu(II) phthalocyanine derived from Alcian Blue. This variant is indicated as a superior alternative to Alcian Blue as for water solubility, staining performance and stability in histologic assays [18]. ABTP is expected to be a G4 binder because of the large dimension of the π system and the presence of four positively charged peripheral substituents. To evaluate the selectivity over double helix DNA (calf thymus DNA) and compare the affinity towards different G4 conformations, mixed/hybrid (Tel23 [19]), antiparallel (CTA22 [20]) and parallel (c-myc [21]) conformations were considered as representative examples. The affinity towards synthetic RNAs (duplex and triplex forms) is in our opinion an interesting but much less studied aspect: it is here investigated as well.
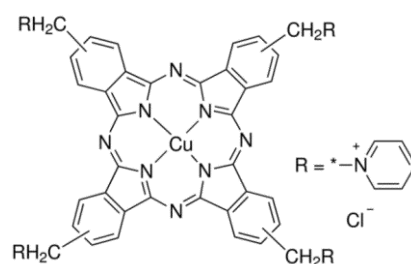

Figure 1. Molecular structure of Alcian Blue-tetrakis(methylpyridinium) chloride (ABTP).

Materials and Methods

Materials

Solid Alcian Blue-tetrakis(methylpyridinium) chloride (ABTP) was purchased from Sigma. Stock solutions of the dye were done by dissolving in water the appropriate amount of the solid; their molar concentration is expressed as C_{ABTP}. Calf thymus DNA (lyophilised sodium salt from Sigma-Aldrich, from now on ct-DNA) was dissolved in water and sonicated, producing short polynucleotide fragments (ca. 500 base pairs) [22, 23]. Stock solutions of ct-DNA were standardized spectrophotometrically ($\varepsilon = 13200$ M^{-1} cm^{-1} at 260 nm, 0.1 M NaCl, pH = 7.0 [24]); concentrations of ct-DNA are expressed in molarity of base pairs and will be indicated as C_{DNA}. Polyriboadenylic·polyribouridylic (polyA·polyU) and polyribouridylic (polyU) acids were purchased from Sigma as potassium salts and the stock solutions were prepared by dissolving suitable amounts of solid in water. The standardization of these synthetic RNA stock solutions was attained spectrophotometrically ($\varepsilon = 14900$ M^{-1} cm^{-1} at 260 nm for polyA·polyU and $\varepsilon = 8900$ M^{-1} cm^{-1} at 260 nm for polyU, at 0.1 M NaCl, pH = 7.0 [25]). PolyA·2polyU triplex was obtained by the quantitative reaction at pH = 7.0 between equimolar amounts of polyU and polyA·polyU [26, 27]. The analytical concentrations of polyA·polyU and polyA·2polyU are expressed in molarity of base pairs and base triplets respectively and indicated as $C_{polyApolyU}$ and $C_{polyA2polyU}$ respectively. Dried DNA oligonucleotides 5'-TAGGGTTAGGGTTAGGGTTAGGG-3' (Tel23 – hybrid, telomeric), 5'-AGGGCTAGGGCTAGGGCTAGGG-3' (CTA22 – antiparallel, telomeric), 5'-TGAGGGTGGGTAGGGTGGGTAA-3' (c-myc – parallel, promoter region of oncogene), were purchased from Metabion. Stock solutions were prepared in aqueous buffers (see below their details) and their molar concentration (in strands) is calculated according to the weight/content provided by the sample certificates. The formation of the G4 structure was carried out by heating oligonucleotide solutions up to 90°C for 6 min and slowly cooling

5

down to room temperature. The solutions were then stored overnight at 4°C. The measurements were performed at 0.1 M NaCl for ct-DNA and 0.1 M KCl for G4. Sodium cacodylate $(CH_3)_2AsO_2Na$ (NaCac, from Sigma Aldrich) 2.5 mM was the pH = 7.0 buffer, whereas lithium cacodylate $(CH_3)_2AsO_2Li$ (LiCac) 2.5 mM was employed in the presence of G4. LiCac was obtained by mixing suitable amounts of aqueous solutions of LiOH and HCac, both from Sigma-Aldrich. Ultra-pure grade water from a SARTORIUS Arium-pro water purification system was used as the reaction medium. All reactants not specifically mentioned were analytical grade and were used without further purifications.

Experimental methods

A Shimadzu UV-2450 spectrophotometer was used to record absorption spectra and to perform spectrophotometric titrations and melting experiments. The apparatus is equipped with a Peltier temperature controller within ± 0.1 °C. In the spectrophotometric titrations, increasing amounts of the titrant were added directly in the cuvette containing the dye and a spectrum was recorded upon each addition. The precise and accurate addition of very small volumes was done owing to a glass syringe connected to a Mitutoyo micrometric screw. The calibration of the delivery system was done by weighting pure water addition in a "Parafilm M"® sealed beaker and yielded 8.20±0.02 µL for a complete turn of the screw; the lowest addition limit is 1/50 of a turn. The melting experiments were carried out by heating the working solutions from 25°C to 90°C with a scan rate of 5°C/min every 6.5 minutes. As c-myc is particularly stable because of its parallel conformation, melting experiments were performed at KCl 10 mM for the ABTP/c-myc system (and 0.1 KCl for other G4). Note that KCl dilution is performed just before c-myc melting experiments whereas folding is done at 0.1 M KCl, and that G4 persistence in the diluted buffer is confirmed *i.a.* by thermal difference spectra and literature data [28]. During the 6.5 minutes, the temperature was kept constant to allow the system to reach the equilibrium. Circular dichroism (CD) spectra were recorded on a MOS-450 spectrophotometer (Bio-

Logic SAS, Claix, France) at 25°C, using a 1.0 cm path-length cell. The buffer baseline was collected and subtracted from the sample spectra.

Results and discussion

Solution studies   Given the known strong tendency of phthalocyanines to undergo auto-aggregation phenomena [6, 29-31], this feature was re-checked here for ABTP under our experimental conditions. In water, absorbance profiles do not seem to change with dye concentration and absorbance vs. concentration plots are linear (Figure S1A-B of the Supporting Information). This behaviour should in principle be against the formation of extended supramolecular structures connected with auto-aggregation phenomena. However, if the band at 500-800 nm is deconvoluted, it might be observed that the shoulder at the right of the maximum increases its contribution to the overall spectrum at the lowest concentrations (Figure S1C). Also, if the absorbance experiments are repeated in ethanol (lower dielectric constant), strong deformations in the shape of the spectrum and changes in the relevant abundance of the two major bands occur by increasing the ABTP content (Figure 2). It can thus be concluded that the band at around λ = 622 nm corresponds to the aggregate, whereas that at about λ = 667 nm should be attributed to the monomer: co-facial H-aggregates are formed. In water, the aggregation process is even stronger than in ethanol [29, 30] and the monomer can hardly be evidenced, even under the most diluted conditions. The shape of the spectra in water corresponds to that in ethanol at the highest ABTP concentrations, indicating that similar types of aggregates are formed. In addition to the main quenching effect due to the central copper ion, the formation of H-aggregates agrees with the absence of any fluorescence emission for the dye solutions [31]. No CD signal is observed for the ABTP solutions in water (Figure S2), but this is in line with the formation of racemic supramolecular structures. Sometimes, aggregates of species

7

like porphyrins may produce CD signals but their chirality can be turned off, depending on the staggering angle [32, 33].
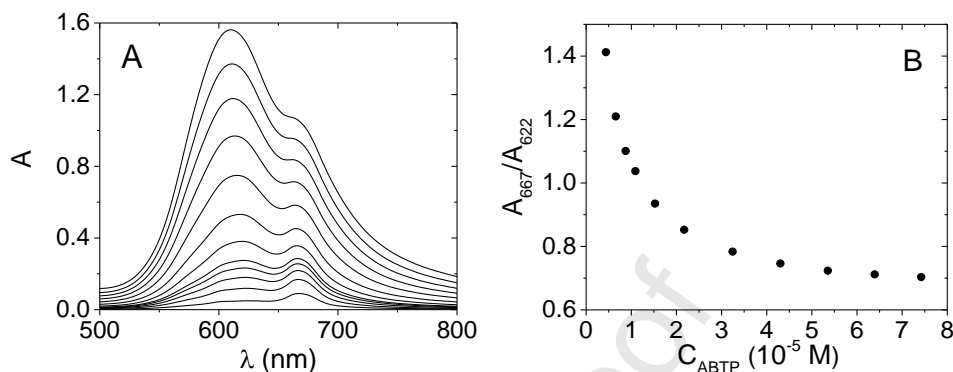

Figure 2 – (A) Absorbance spectra of ABTP in ethanol and (B) A_{667}/A_{622} ratios at different dye concentrations. C_{ABTP} from 2.19×10^{-6} M to 7.42×10^{-5} M, NaCl 0.1 M, NaCac 2.5 mM, pH 7.0, T = 25.0 °C.

Binding to polynucleotides ABTP was first investigated as for affinity towards a natural polynucleotide as ct-DNA and synthetic RNAs (double-stranded polyA·polyU and triple-stranded polyA·2polyU) through absorbance titrations. Figure 3 and Figure S3 show the absorbance spectra recorded during spectrophotometric titrations where known amounts of ct-DNA, polyA·polyU or polyA·2polyU are added to an ABTP solution. Although the spectral changes are not very remarkable, the interactions are well confirmed by the appearance of a peak at $\lambda = 682$ nm. The similarity both in the shape and in the wavelength of this peak constitutes an indication that ABTP binds to the biosubstrate as a monomer and that binding favours aggregates' disruption. This agrees with the fact that in particular in the presence of high binding site amounts, the dye will distribute itself over them. A similar effect was demonstrated for the DNA binding of the monomer in systems with aggregating dyes [34, 35]. The binding isotherm of the titrations is biphasic, with a sharp initial change followed by a smoother curve. This is in keeping with some aggregation of

8

the dye on the polymer surface for the first points, i.e. those in the presence of high dye excess. Oppositely, when the polynucleotide is the major species, its interaction with the dye monomer is the predominant process.
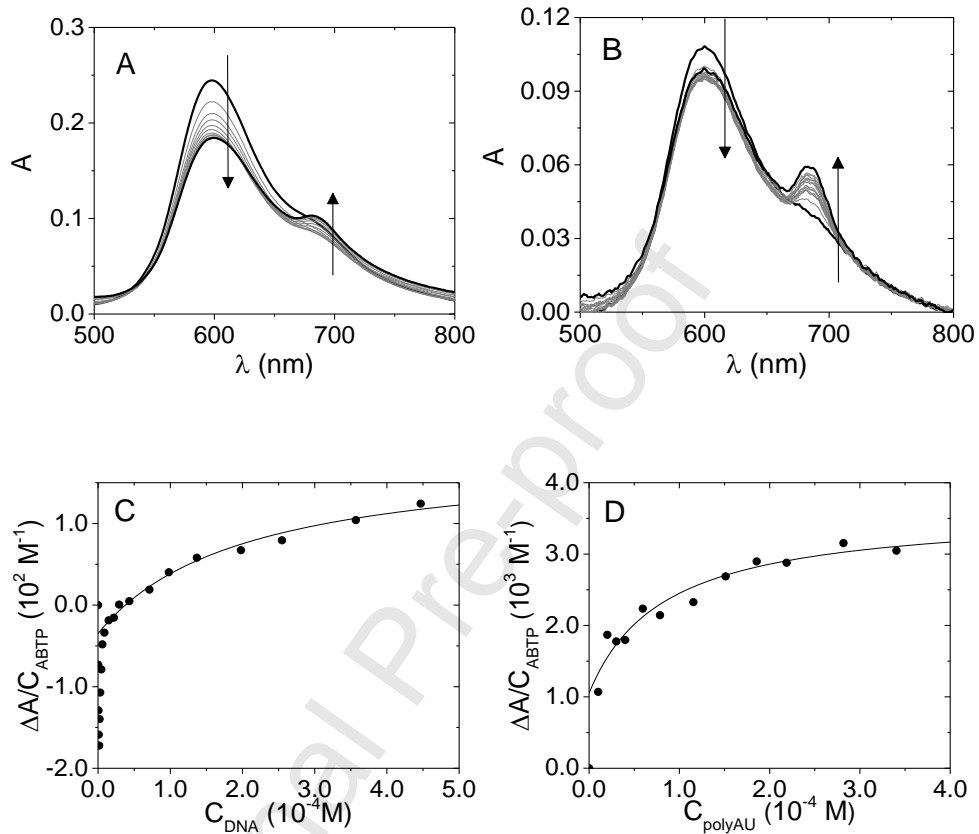

Figure 3 – Spectrophotometric titration of (A) ABTP/ct-DNA ($C_{ABTP} = 8.73 \times 10^{-6}$ M, C_{DNA} from 0 M to 4.47×10^{-4} M) and (B) ABTP/polyApolyU ($C_{ABTP} = 4.32 \times 10^{-6}$ M, $C_{polyApolyU}$ from 0 M to 3.41×10^{-4} M). Relevant binding isotherms are shown in panels (C) and (D) respectively ($\lambda = 682$ nm). NaCl 0.1 M, NaCac 2.5 mM, pH 7.0, T = 25.0 °C. Continuous line is data fitting according to Eq. (4).

A general reaction scheme can be that below (Eqs. (1-2)).

$$P + D \quad \leftrightarrows \quad PD \tag{1}$$

$$\updownarrow +(m-1)D \qquad \updownarrow +(m-1)D$$

$$P + D_m \quad \leftrightarrows \quad PD_m \tag{2}$$

9

This system might be expressed by the apparent reaction

$$P + D_f \rightleftarrows PD_T \tag{3}$$

where P is the polynucleotide (in base pairs or triplets for polyA·2polyU), D_f considers any form of free dye ($[D_f] = [D] + m[D_m]$), PD_T is the total of bound species ($[PD_T] = [PD] + [PD_m]$) and K_{app} is the binding constant related to this model. To perform an analysis of the DNA binding, only the points related to polynucleotide excess are taken into account. Under these circumstances $[PD_m]$ can be supposed to be a minority and $K_{app} = \alpha_D \times K$ where $\alpha_D = [D]/[D_f]$ is the monomer fraction and K is the equilibrium constant for monomer binding only (Eq. (1)). K_{app} can be evaluated by interpolating the data points at $C_{DNA} > C_{ABTP}$ using Eq. (4) [35-37].

$$\Delta A/C_{ABTP} = (K_{app}\Delta\varepsilon[P])/(1+K_{app}[P]) + k \tag{4}$$

In Eq. (4), [P] is the free polynucleotide content, $\Delta A = A - \varepsilon_{ABTP}C_{ABTP}$ is the amplitude of the binding isotherm, and k is an offset. Initially, the total concentration of the polymer is introduced in Eq. (4) in place of [P] to obtain a first K_{app} estimation that can be used to calculate $[P] = C_P - [PD]$. Then, K_{app} is re-evaluated and the procedure is repeated until convergence is reached. The continuous lines in Figures 3C-D are relevant to the fitting procedure. In NaCl 0.1 M, NaCac 2.5 mM, pH 7.0 and 25 °C we have K_{app}(ABTP/ct-DNA) = $(5.0 \pm 1.1) \times 10^3$ M^{-1}, K_{app}(ABTP/polyA·polyU) = $(1.2 \pm 0.6) \times 10^4$ M^{-1} and K_{app}(ABTP/polyA·2polyU) = $(6.2 \pm 3.2) \times 10^3$ M^{-1}. The titrations for the ABTP/DNA system were repeated at different temperatures in the 15 – 46 °C range. Figure 4 shows the dependence of K_{app} on the temperature for all the systems analysed.
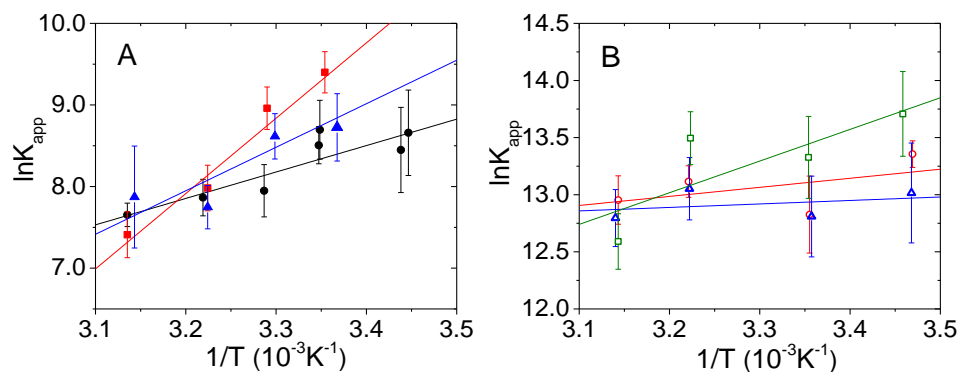
10

Figure 4 – Dependence of K_{app} on temperature for the ABTP/ct-DNA (●), ABTP/polyA·polyU (■), ABTP/polA·2polyU (▲) systems related to polynucleotides (A, NaCl 0.1 M, NaCac 2.5 mM, pH 7.0) and for ABTP/Tel23 (○), ABTP/c-myc (Δ) and ABTP/CTA22 (◻) systems with oligonucleotides (B, KCl 0.1 M, LiCac 2.5 mM, pH 7.0).

For ABTP/ct-DNA, the process is found to be exothermic with $\Delta H_{app} = - 22 \pm 6$ kJ/mol. The slope of the van't Hoff's plots is higher for the RNAs ($\Delta H_{app} = - 77 \pm 8$ kJ/mol for ABTP/polyA·polyU and $\Delta H_{app} = - 44 \pm 14$ kJ/mol for ABTP/polyA·2polyU). This order of magnitude for enthalpy changes lies at the boundaries between groove binding (low negative or positive ΔH) and intercalation (highly negative ΔH) [38, 39]. Figure 5 shows an enthalpy/entropy compensation (EEC) plot [40, 41] for the studied systems, which will be better discussed below. We have to keep in mind that these parameters are apparent ones, due to the coupling with the dye-dye aggregation process. However, they can still provide information on the dye-biosubstrate binding process. Indeed, being aggregation contribution the same in all systems, they suggest different binding features between RNA polynucleotides and natural DNA. This is confirmed by melting experiments. In the case of the ABTP/ct-DNA system, precipitation phenomena occurring by increasing the temperature above a certain threshold do not enable to register a complete melting curve.
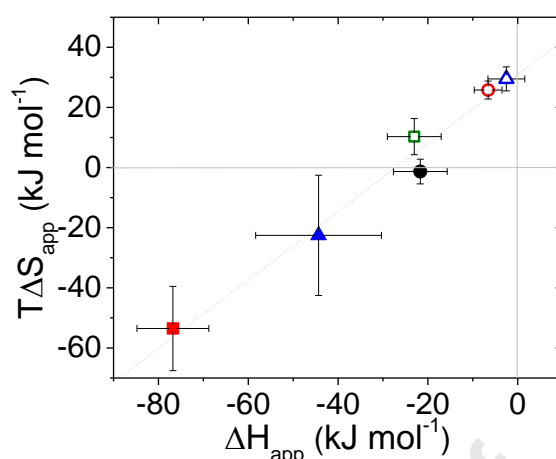
11

Figure 5 – Enthalpy-entropy compensation (EEC) plot for the studied systems (T = 25.0 °C); ABTP/ct-DNA (●), ABTP/polyA·polyU (■), ABTP/polA·2polyU (▲) (NaCl 0.1 M, NaCac 2.5 mM, pH 7.0); ABTP/Tel23 (○), ABTP/c-myc (△) and ABTP/CTA22 (▣) (KCl 0.1 M, LiCac 2.5 mM, pH 7.0).

On the contrary, melting studies are possible for both ABTP/polyA·polyU and ABTP/polyA·2polyU systems, which showed significant helix stabilisation upon ABTP binding (at C_{ABTP}/C_{poly} = 1.25, ΔT_m > 15°C for both ABTP/polyA·polyU and ABTP/polyA·2polyU systems, Figure S4). Circular dichroism (CD) titrations (Figure 6 and Figure S5) confirm the very different behaviour of DNA vs. RNA. For ct-DNA, a significant induced CD (ICD) negative signal appears in the visible region upon dye addition to the polymer, which indicates that the DNA interaction induces a supramolecular order on ABTP. The amplitude the ICD signal corresponds to $|\Delta\varepsilon|$ = 4.7 M^{-1}cm^{-1}, a value which is compatible with an intercalative process ($|\Delta\varepsilon|$ < 10 M^{-1}cm^{-1} [42, 43]). The interaction with RNAs does not produce the same effect and no ICD bands are present.

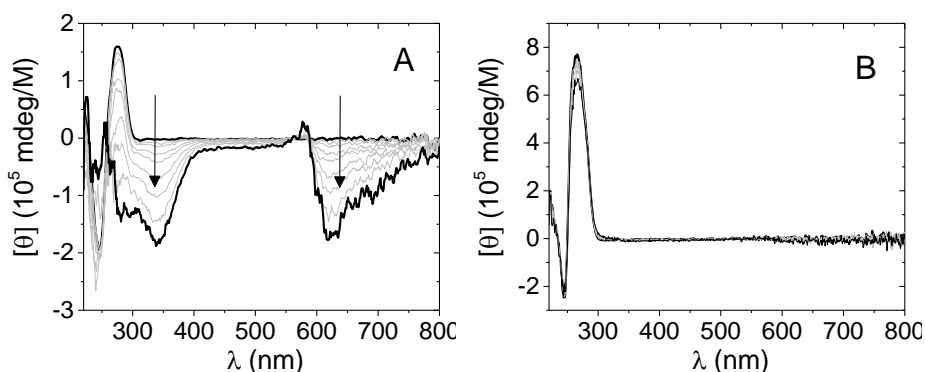**Figure 6** – CD spectra of (A) ABTP/ct-DNA ($C_{DNA} = 1.05 \times 10^{-4}$ M, C_{ABTP} from 0 M to 9.77×10^{-5} M), (B) ABTP/ polyA·polyU ($C_{polyApolyU} = 7.75 \times 10^{-5}$ M, C_{ABTP} from 0 M to 3.33×10^{-5} M). NaCl 0.1 M, NaCac 2.5 mM, pH 7.0; T = 25.0 °C

The different conformation of the polynucleotides for sure plays a major role in driving the binding features. It is known that natural DNA adopts a conformation called B-DNA, while RNAs structure (both in the double and triple helix form) closely corresponds to a geometry called A-DNA [44, 45]. In RNA duplexes, the displacement of the base pairs from the helical axis is considerable, with the base plane tilted away from the plane vertical to the axis; thus, intercalation of a large porphyrin molecule should be disfavoured. A-DNA is characterized by a broad shallow minor groove and a deep narrow major groove, and the phosphate groups locate closer [44, 46]. The binding to the minor groove would neutralize the negative charge on the phosphates, and the groove is now wide enough to accommodate the ABTP molecule. Similar behaviour was already found, for instance for meso-tetrakis(N-methylpyridinium-4-yl)porphyrin [46]. Even if the significant stabilisation of the RNAs could, at first sight, be against external/groove binding, similar ΔT_m can be found also for this binding mode [45] and would agree with the stabilising effect of a +4 charges species whose presence strongly reduces phosphates repulsion. On the contrary, the geometrical parameters would not be similarly favourable in the case of DNA: here the evident ICD negative bands strongly indicate an intercalative process. Being ABTP a

13

particularly extended molecule, partial intercalation is the more probable option due to geometrical constraints. It might be speculated that the outside protruding part could constitute a bridge for some strand-strand aggregating process (being also the inter-DNA repulsion lowered by positive ABTP); the possible formation of higher order adducts as double helix-double helix ones, stabilised by dye bridges, is a process which was found to be enhanced at higher temperature [47]. This might be the reason for precipitation during the ABTP/ct-DNA melting tests.

G-quadruplex ABTP was tested for affinity to different G-quadruplex (G4) structures. The G4 chosen all contain three G-tetrads but have different conformations (Figure 7), being this hybrid in the case of Tel23, antiparallel for CTA22 and parallel for c-myc [48].
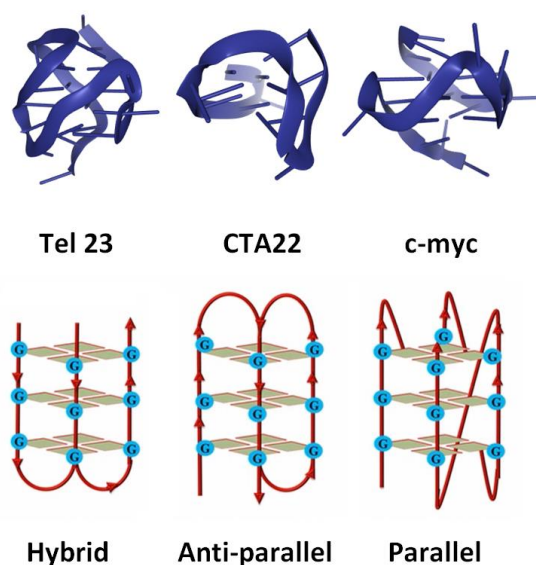

Figure 7 – Conformations of the different G-quadruplexes (G4) used in this work; G4 structure (ribbon rendering, above) is from Protein data bank, the sketches of the relevant conformations are shown below.

The relevance of the spectral changes immediately suggests a strong affinity for all the G4 (Figure 8 and Figure S6): the band of the adduct (peaked at around $\lambda = 690$ nm) is much more prominent than in the case of the polynucleotides.
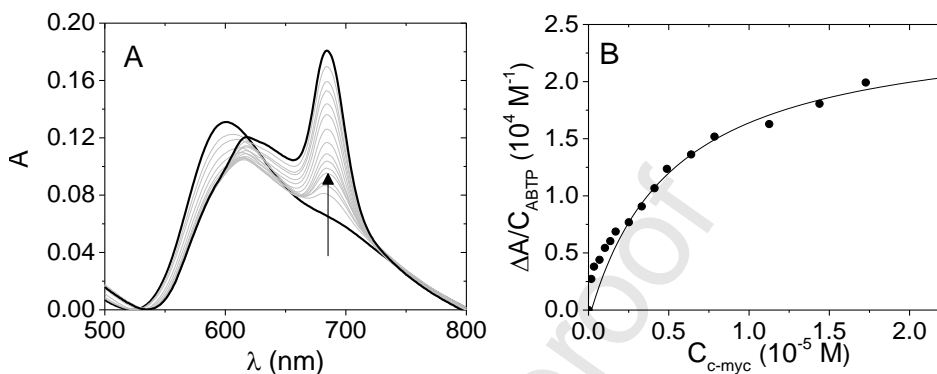

Figure 8 – (A) Spectrophotometric titration ABTP/ c-myc and (B) relevant binding isotherm at $\lambda = 690$ nm. $C_{ABTP} = 5.46 \times 10^{-6}$ M, C_{c-myc} from 0 M to 1.73×10^{-5} M, KCl 0.1 M, LiCac 2.5 mM, pH 7.0, T = 25.0 °C; continuous line is data fitting according to Eq. (4).

Eq. (4) can again be used to evaluate K_{app} for the binding process. At 25.0 °C we have $K_{app}(ABTP/Tel23) = (3.7 \pm 1.2) \times 10^5$ M^{-1}, $K_{app}(ABTP/c-myc) = (3.6 \pm 1.1) \times 10^5$ M^{-1} and $K_{app}(ABTP/CTA22) = (6.1 \pm 2.1) \times 10^5$ M^{-1} (KCl 0.1 M, LiCac 2.5 mM, pH 7.0). Despite the high errors, it seems that the affinity for CTA22 is somewhat higher, as also evidenced in Figure 4B. Also, note that at the end of titration (same C_{G4}/C_{ABTP}) the ratio between the two major peaks is around 1.0 for ABTP/CTA22 and 1.5 for both ABTP/Tel23 and ABTP/c-myc (Figure 9A). The spectrophotometric behaviour will be the result of the type of binding and relevant affinity, together with the coupling with dye-dye aggregation effects. At constant temperature, given the identical starting dye content (C_{ABTP}) and similar biosubstrates, differences in the shapes of the spectrum of the bound species might suggest subtle differences in the bound forms. On the other hand, a significant increase of the binding isotherm amplitude on increasing temperature is observed (Figure 9B), which

15

should be correlated not only to the dependence of K_{app} on T but also to the contribution of a different dye aggregation extent.
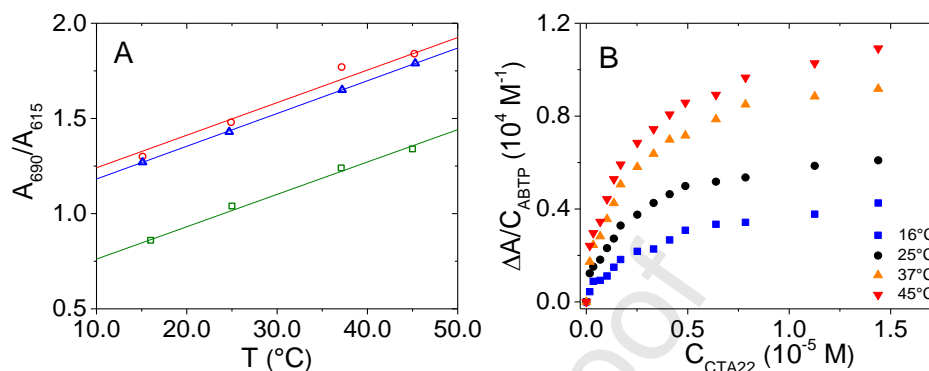

Figure 9 – (A) Ratio between the absorbance of the two main peaks of ABTP/Tel23 (○), ABTP/CTA22 (■) and ABTP/c-myc (△) at the end of the spectrophotometric titration and (B) dependence of the binding isotherm amplitude (λ = 690 nm) on temperature for ABTP/CTA22 (KCl 0.1 M, LiCac 2.5 mM, pH 7.0)

In the case of G4, the process is even less exothermic than what observed for natural DNA (ΔH_{app} = - 6.6 ± 3.1 kJ/mol for ABTP/Tel23; ΔH_{app} = - 23 ± 6 kJ/mol for ABTP/CTA22; ΔH_{app} = - 2.5 ± 4.1 kJ/mol for ABTP/c-myc). These low values agree with a picture where the dye will be externally bound. G4s are stable and rigid structures, whose distortion requires a very high energy cost: stacking of the drug on the outer planes of tetrads is often a more probable mode for ligands whereas deep intercalation is a difficult event [49]. In the case of CTA22, some slightly higher interaction with the internal bases might be at play (higher ΔH_{app}), due to subtle differences in the geometrical factors (Figure 7). External binding is also confirmed by the thermal denaturation tests. The melting plots at λ = 295 nm [50] are reported in Figure S7. No stabilisation is observed for the ABTP-G4 complexes compared to that of G4 alone, meaning that no relevant structural modification

16

has occurred. The melting process of the ABTP-G4 complexes turns out to be reversible, with perfect superimposition between the folding and the unfolding mechanism (Figure S8). This means that the presence of ABTP does not affect the G4 structures folding, which can come back to their starting conformation. Thermal difference spectra, i.e. the difference between final and initial spectrum during melting tests, constitute a signature for G4 structure [51]. Figure S9 contains the thermal difference spectra of the here analysed systems and confirms: (i) that the three G4 have different geometries; (ii) that these geometries are not significantly modified in the presence of ABTP.

Some speculative discussion on the reasons for the non-identical features of the ABTP-G4 complexes might be done. The extended inner π-system of phthalocyanines is 1.0 nm wide, and the G-tetrad is 1.5 nm [16]. Therefore, in principle, the geometrical constraint for ABTP/G4 surface interaction is nicely fulfilled. However, stacking at the top tetrad is a process which should have produced high thermal stabilisation and which needs a sequence providing a free top surface [17]. This binding mode does not seem to be the preferred one for the present systems. The possible selectivity towards a particular conformation can be due to the different distortion of the tetrad (for parallel conformations planarity is higher), which is a function not only of the sequence but also of the coordinated metal ion [16]. In the different G4 geometries, the G-tetrad is differently hindered by the loops and the lateral surfaces are differently free/exposed (Figure 7). The affinity for the negatively charged loops might be at play in particular if the phthalocyanine core is functionalised with positively charged residues as in the case of ABTP.

Interestingly, the thermodynamic parameters for G4s obtained using the van't Hoff plots shown in Figure 4B, are in line with the general enthalpy-entropy compensation (EEC) plot for ABTP (Figure 5). EEC has been widely observed and reported for protein-ligand interactions but also other biosubstrates such as DNA [40, 52, 53]. EEC is a debated phenomenon which, in some cases, has been attributed to experimental errors and

17

limitations or a natural consequence of thermodynamics [54]. However, there is now much clear evidence of EEC: it is typically explained by assuming that if a molecular change in the ligand leads to more and/or tighter van der Waals contacts and H-bonds with the substrate (giving a more negative enthalpy change, ΔH), this inevitably leads to reduced mobility/flexibility in either or both components of the interaction, i.e., a reduction in the overall conformational entropy, and that change compensates the enthalpy decrease [55]. The importance of the rearrangement of water molecules and different hydration has also been evidenced [53, 55]. These effects would be the ones which drive the entropy change (TΔS$_{app}$) to be able to change from positive to negative values (Figure 5). Despite the somehow high errors on the thermodynamic values, the correlation plot for the ABTP may be assumed to be linear. The slope close to one indicates that the enthalpy gain from the complexation is cancelled out by the entropic loss from the conformational changes caused upon binding (rigid hosts will correspond to much lower slopes [56]). The intercept of the plot is associated with the degree of desolvation upon binding. Its value is high (around 30 kJ mol^{-1}) and very close to the value found in the case of the interaction of a zinc porphyrin to diamines [56].

Conclusions

The here analysed systems are complicated by the superimposition of auto-aggregation effects for the ABTP phthalocyanine. However, under biosubstrate excess conditions and referring to the apparent reaction, we can still gain information on the different mechanistic aspects of the binding process. ABTP binds to all biosubstrates but with different features. Interaction with both double and triple-stranded RNAs exists and occurs differently to ct-DNA. The point of structure-specific nucleic acid-interactive drugs based on the

geometrical features is a very interesting but complex aspect. In these complicate systems, a subtle change in the geometry can have important effects on the binding mode, mixed binding modes are at play and, also, different binding features could become majority depending on the experimental conditions (for instance reagents concentrations) [45, 57]. In the case of RNAs external/groove binding is the found active mode. The presence of a wide and swallow minor groove in these A-type polynucleotides could drive external interaction of the wide structure of ABTP. The absence of a precise orientation on the helix surface agrees with the absence of ICD signals. Also, given that the +4 charge of ABTP on the surface can balance the phosphates repulsion, this is in line with the significant stabilization found in the ABTP/RNAs melting experiments. On the other hand, in the case of ct-DNA, the CD experiments strongly indicate dye intercalation. Geometrical constraints support half intercalation which, in turn, would favour inter-strand precipitation by increasing temperature over a certain threshold (melting experiments). The thermodynamic parameters are difficult to discuss and compare from a strictly numerical point of view in particular due to the superimposition of aggregation effects. However, they confirm the different behaviour between RNAs and DNA. Also, all parameters belong to the same line in an EEC plot indicating the consistency of the different ABTP systems. The dye has a complex reactivity, which considers both intercalation and groove/external binding and where the thermodynamic aspects of these two possibilities can be differently balanced in the presence of the different (but always nucleotide-based) biosubstrates. ABTP can externally bind to the analysed G4s. Even if more often authors claim selectivity towards parallel forms, this is not always the case. For instance, for N-methyl mesoporphyrin both preference for parallel [58] or anti-parallel [59] G4 sequences was demonstrated. In the here presented work, beyond a general affinity for all G4s, ABTP seems to (slightly) prefer CTA22 antiparallel telomeric form, to which it binds differently

19

from the very similar features of the ABTP/Tel23 (hybrid) and ABTP/c-myc (parallel) systems.

Acknowledgements

List of abbreviations

ABTP = Alcian Blue-tetrakis(methylpyridinium) chloride, copper phthalocyanine, +4 charge

C_{ABTP} = ABTP molar concentration

CD = circular dichroism

c-myc = 5'-TGAGGGTGGGTAGGGTGGGTAA-3', 22-mer DNA oligonucleotide, parallel, promoter region of oncogene.

$C_{polyApolyU}$ = polyA·polyU molar concentration in base pairs

$C_{polyA2polyU}$ = polyA·2polyU molar concentration in base triplets

CTA22 = 5'-AGGGCTAGGGCTAGGGCTAGGG-3', 22-mer DNA oligonucleotide, antiparallel, telomeric

DNA, ct-DNA = natural DNA, double stranded, B-form from calf thymus

EEC = enthalpy-entropy compensation

G4 = G-quadruplex of the DNA type

poly(A)·poly(U) = double stranded synthetic RNA, poly(rA)·poly(rU)

poly(A)·2poly(U) = triple stranded synthetic RNA, poly(rA)·2poly(rU)

RNA = here intended as synthetic polynucleotide, might be either poly(rA)·poly(rU) double strand or poly(rA)·2poly(rU) triple strand

Tel 23 = 5'-TAGGGTTAGGGTTAGGGTTAGGG-3', 23-mer DNA oligonucleotide, hybrid, telomeric.

Bibliographic references

[1] G. Loebbert Journal (2002) Pages.

[2] S.Q. Lomax, Studies in Conservation, vol. 50, Routledge, 2005, pp. 19-29.

[3] J.E. Scott, J. Dorling, Histochemie, vol. 5, 1965, pp. 221-233.

[4] J.E. Scott, Histochemie, vol. 37, 1973, pp. 379-380.

[5] J.E. Scott, Histochemie, vol. 32, 1972, pp. 191-212.

[6] J.E. Scott, Histochemie, vol. 21, 1970, pp. 277-285.

[7] L.B. Josefsen, R.W. Boyle, Theranostics, vol. 2, Ivyspring International Publisher, 2012, pp. 916-966.

[8] M. Machacek, A. Cidlina, V. Novakova, J. Svec, E. Rudolf, M. Miletin, R. Kučera, T. Simunek, P. Zimcik, Journal of Medicinal Chemistry, vol. 58, American Chemical Society, 2015, pp. 1736-1749.

[9] N. Sekkat, H. van den Bergh, T. Nyokong, N. Lange, Molecules, vol. 17, MDPI, 2011, pp. 98-144.

[10] T. Arslan, M. Bugrahan Ceylan, H. Bas, Z. Biyiklioglu, M. Senturk, Dalton Trans., vol. 49, Royal Society of Chemistry, 2020, pp. 203-209.

[11] N.A. Kasyanenko, R.A. Tikhomirov, V.M. Bakulev, V.N. Demidov, E.V. Chikhirzhina, E.B. Moroshkina, ACS Omega, vol. 4, American Chemical Society, 2019, pp. 16935-16942.

[12] T. Keles, B. Barut, A. Ozel, Z. Biyiklioglu, Dyes Pigm., vol. 164, Elsevier Ltd., 2019, pp. 372-383.

[13] L.E. Xodo, S. Cogoi, V. Rapozzi, Future Med. Chem., vol. 8, Future Science Ltd., 2016, pp. 179-194.

[14] A. De Cian, L. Lacroix, C. Douarre, N. Temime-Smaali, C. Trentesaux, J.-F. Riou, J.-L. Mergny, Biochimie, vol. 90, 2008, pp. 131-155.

[15] S. Neidle, Nature Reviews Chemistry, vol. 1, 2017, pp. 0041.

[16] H. Yaku, T. Fujimoto, T. Murashima, D. Miyoshi, N. Sugimoto, Chemical Communications, vol. 48, The Royal Society of Chemistry, 2012, pp. 6203-6216.

[17] J. Lopes-Nunes, J. Carvalho, J. Figueiredo, C.I.V. Ramos, L.M.O. Lourenço, J.P.C. Tomé, M.G.P.M.S. Neves, J.-L. Mergny, J.A. Queiroz, G.F. Salgado, C. Cruz, Bioorganic Chemistry, vol. 100, 2020, pp. 103920.

[18] C.J. Churukian, M. Frank, R.W. Horobin, Biotechnic & Histochemistry, vol. 75, Taylor & Francis, 2000, pp. 147-150.

[19] C. Bazzicalupi, M. Ferraroni, F. Papi, L. Massai, B. Bertrand, L. Messori, P. Gratteri, A. Casini, Angewandte Chemie International Edition, vol. 55, 2016, pp. 4256-4259.

[20] K.W. Lim, P. Alberti, A. Guédin, L. Lacroix, J.-F. Riou, N.J. Royle, J.-L. Mergny, A.T. Phan, Nucleic Acids Res, vol. 37, Oxford University Press, 2009, pp. 6239-6248.

[21] A. Ambrus, D. Chen, J. Dai, R.A. Jones, D. Yang, Biochemistry, vol. 44, American Chemical Society, 2005, pp. 2048-2058.

[22] T. Biver, F. Secco, M.R. Tine, M. Venturini, A. Bencini, A. Bianchi, C. Giorgi, Journal of Inorganic Biochemistry, vol. 98, 2004, pp. 1531-1538.

[23] F. Macii, G. Salvadori, R. Bonini, S. Giannarelli, B. Mennucci, T. Biver, Spectrochimica Acta Part A: Molecular and Biomolecular Spectroscopy, vol. 223, 2019, pp. 117313.

[24] G. Felsenfeld, S.Z. Hirschman, Journal of Molecular Biology, vol. 13, 1965, pp. 407-427.

[25] T. Biver, N. Busto, B. Garcìa, J.M. Leal, L. Menichetti, F. Secco, M. Venturini, Journal of Inorganic Biochemistry, vol. 151, 2015, pp. 115-122.

[26] B. Garcia, J.M. Leal, V. Paiotta, S. Ibeas, R. Ruiz, F. Secco, M. Venturini, The Journal of Physical Chemistry B, vol. 110, American Chemical Society, 2006, pp. 16131-16138.

[27] F.J. Hoyuelos, B. García, J.M. Leal, N. Busto, T. Biver, F. Secco, M. Venturini, Physical Chemistry Chemical Physics, vol. 16, The Royal Society of Chemistry, 2014, pp. 6012-6018.

[28] M.M. Islam, S. Fujii, S. Sato, T. Okauchi, S. Takenaka, Molecules, vol. 20, 2015.

[29] H. Isago, H. Fujita, Journal of Porphyrins and Phthalocyanines, vol. 22, 2018, pp. 102-111.

[30] M.A. Rauf, S. Hisaindee, J.P. Graham, M. Nawaz, Journal of Molecular Liquids, vol. 168, 2012, pp. 102-109.

[31] M. Bayda, F. Dumoulin, G.L. Hug, J. Koput, R. Gorniak, A. Wojcik, Dalton Transactions, vol. 46, The Royal Society of Chemistry, 2017, pp. 1914-1926.

[32] K. Kadish, R. Guilard, K. Smith (Eds.), The Porphyrin Handbook vol 18: Multporphyrins, Multiphthalocyanines and Arrays, Elsevier, 2012.

[33] N. Berova, L.D. Bari, G. Pescitelli, Chemical Society Reviews, vol. 36, The Royal Society of Chemistry, 2007, pp. 914-931.

[34] T. Biver, A. Boggioni, F. Secco, E. Turriani, M. Venturini, S. Yarmoluk, Archives of biochemistry and biophysics, vol. 465, 2007, pp. 90-100.

[35] T. Biver, N. Eltugral, A. Pucci, G. Ruggeri, A. Schena, F. Secco, M. Venturini, Dalton Transactions, vol. 40, The Royal Society of Chemistry, 2011, pp. 4190-4199.

[36] T. Biver, A. Corti, N. Eltugral, E. Lorenzini, M. Masini, A. Paolicchi, A. Pucci, G. Ruggeri, F. Secco, M. Venturini, Journal of Nanoparticle Research, vol. 14, 2012, pp. 681.

[37] S. Biagini, A. Bianchi, T. Biver, A. Boggioni, I.V. Nikolayenko, F. Secco, M. Venturini, Journal of Inorganic Biochemistry, vol. 105, 2011, pp. 558-562.

[38] J.B. Chaires, Archives of Biochemistry and Biophysics, vol. 453, 2006, pp. 26-31.

[39] R.M. Kenney, K.E. Buxton, S. Glazier, Biophysical Chemistry, vol. 216, 2016, pp. 9-18.

[40] X. Qu, J. Ren, P.V. Riccelli, A.S. Benight, J.B. Chaires, Biochemistry, vol. 42, American Chemical Society, 2003, pp. 11960-11967.

[41] B. García, J.M. Leal, R. Ruiz, T. Biver, F. Secco, M. Venturini, The Journal of Physical Chemistry B, vol. 114, American Chemical Society, 2010, pp. 8555-8564.

[42] B. Nordén, T. Kurucsev, Journal of Molecular Recognition, vol. 7, 1994, pp. 141-155.

[43] T. Biver, Applied Spectroscopy Reviews, vol. 47, Taylor & Francis, 2012, pp. 272-325.

[44] S. Neidle, L.H. Pearl, J.V. Skelly, Biochemical Journal, vol. 243, 1987, pp. 1-13.

[45] W.D. Wilson, L. Ratmeyer, M. Zhao, L. Strekowski, D. Boykin, Biochemistry, vol. 32, American Chemical Society, 1993, pp. 4098-4104.

[46] T. Uno, K. Hamasaki, M. Tanigawa, S. Shimabayashi, Inorganic Chemistry, vol. 36, American Chemical Society, 1997, pp. 1676-1683.

[47] C. Qin, F. Kang, W. Zhang, W. Shou, X. Hu, Y. Gao, Water Research, vol. 123, 2017, pp. 58-66.

[48] N. Busto, P. Calvo, J. Santolaya, J.M. Leal, A. Guédin, G. Barone, T. Torroba, J.-L. Mergny, B. García, Chemistry – A European Journal, vol. 24, 2018, pp. 11292-11296.

[49] T.-m. Ou, Y.-j. Lu, J.-h. Tan, Z.-s. Huang, K.-Y. Wong, L.-q. Gu, ChemMedChem, vol. 3, 2008, pp. 690-713.

[50] J.-L. Mergny, A.-T. Phan, L. Lacroix, FEBS Letters, vol. 435, 1998, pp. 74-78.

[51] J.-L. Mergny, J. Li, L. Lacroix, S. Amrane, J.B. Chaires, Nucleic Acids Res, vol. 33, 2005, pp. e138-e138.

[52] S.-R. Tzeng, C.G. Kalodimos, Biophysical Reviews, vol. 7, 2015, pp. 251-255.

[53] A.I. Dragan, C.M. Read, C. Crane-Robinson, European Biophysics Journal, vol. 46, 2017, pp. 301-308.

[54] K. Sergei, Current Protein & Peptide Science, vol. 19, 2018, pp. 1088-1091.

[55] U. Ryde, MedChemComm, vol. 5, The Royal Society of Chemistry, 2014, pp. 1324-1336.

[56] K. Wada, T. Mizutani, H. Matsuoka, S. Kitagawa, Chemistry – A European Journal, vol. 9, John Wiley & Sons, Ltd, 2003, pp. 2368-2380.

[57] M.R. Beccia, T. Biver, A. Pardini, J. Spinelli, F. Secco, M. Venturini, N. Busto Vázquez, M.P. Lopez Cornejo, V.I. Martin Herrera, R. Prado Gotor, Chemistry – An Asian Journal, vol. 7, John Wiley & Sons, Ltd, 2012, pp. 1803-1810.

[58] J.M. Nicoludis, S.P. Barrett, J.-L. Mergny, L.A. Yatsunyk, Nucleic Acids Res, vol. 40, 2012, pp. 5432-5447.

[59] D. Zhao, X. Dong, N. Jiang, D. Zhang, C. Liu, Nucleic Acids Res, vol. 42, 2014, pp. 11612-11621.

Declaration of interests

☒ The authors declare that they have no known competing financial interests or personal relationships that could have appeared to influence the work reported in this paper.

☐The authors declare the following financial interests/personal relationships which may be considered as potential competing interests:

FIGURE
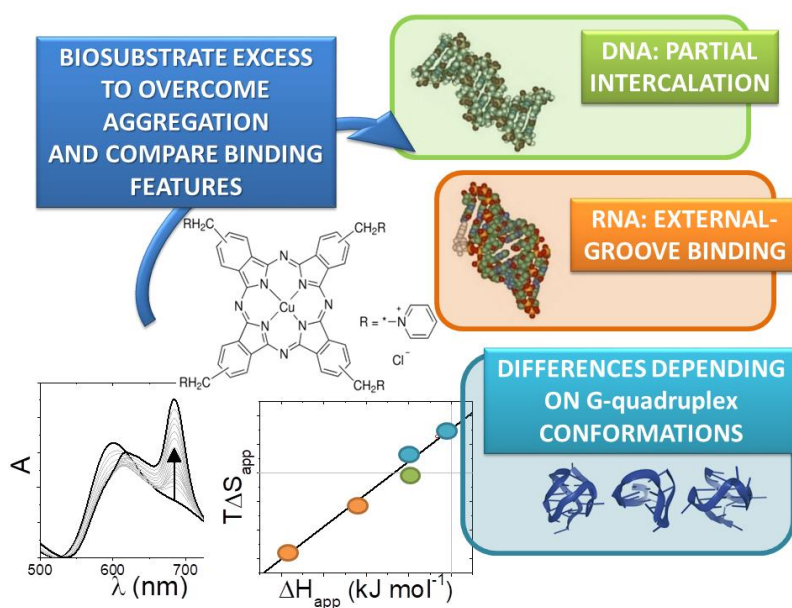
SYNOPSIS

We analysed copper phthalocyanine (Alcian Blue-tetrakis(methylpyridinium) chloride, ABTP) monomer binding using apparent parameters and biosubstrate excess. RNAs shallow and wide grooves favour external binding. For DNA half-intercalation prevails, likely producing inter-strand links. G-quadruplexes are externally bound without geometrical change. ABTP slightly prefers anti-parallel forms. The studied systems undergo enthalpy-entropy compensation.

HIGHLIGHTS

- Copper phthalocyanine Alcian Blue-tetrakis(methylpyridinium) chloride (ABTP) was studied

- Polynucleotide's geometry strongly influences ABTP binding mode

- RNA's wide and swallow minor groove favours ABTP external/groove binding

- DNA half-intercalation might produce even inter-strand binding and precipitation

- ABTP differently binds to anti-parallel G-quadruplex forms